Scripta Materialia 226 (2023) 115236

Contents lists available at ScienceDirect

Scripta Materialia

journal homepage: www.journals.elsevier.com/scripta-materialia

Substantially strengthening a dual-phase titanium alloy by moderate oxygen doping

Yu Fu [a], Wenlong Xiao [a,b,*], Shiteng Zhao [a], Lei Ren [a,c], Junshuai Wang [a], Jian Rong [a], Juan Li [d], Xinqing Zhao [a], Chaoli Ma [a,b]

[a] Key Laboratory of Aerospace Advanced Materials and Performance of Ministry of Education, School of Materials Science and Engineering, Beihang University, Beijing 100191, China
[b] Yunnan Innovation Institute of Beihang University, Kunming 650000, China
[c] Key Laboratory of Mechanics in Fluid Solid Coupling Systems, Institute of Mechanics, Chinese Academy of Sciences, Beijing 100190, China
[d] AECC Beijing Institute of Aeronautical Materials, Beijing 100095, China

ARTICLE INFO

Keywords:
Titanium alloy
Equiaxed microstructure
Interstitial oxygen
High strength
Deformation mechanisms

ABSTRACT

As one of the detrimental ingredients, oxygen can, even in a small amount, substantially reduce the ductility of Ti alloys. Here, rather than being discouraged by the negative effects of oxygen on ductility, an equiaxed dual-phase Ti-8Nb-2Fe-0.66O (wt.%) alloy showing ultrahigh yield strength (1386 MPa) and good tensile ductility (fracture elongation ~10.8%) was developed. The oxygen-containing alloy is 87% stronger than the oxygen-free base alloy whereas the ductility loss is marginal. The effects of oxygen interstitials can be twofold: they led to significant solid-solution strengthening by pinning dislocations and suppressing stress-induced martensitic transformation; the equiaxed α + β dual-phase with basal α texture doped by oxygen promoted multiple ⟨***c*** + ***a***⟩-type and ⟨***a***⟩-type dislocation activities that guaranteed good ductility. This work demonstrates a new avenue to develop high-strength Ti alloys by doping oxygen interstitials, which takes full advantage of the beneficial strengthening factor of oxygen while avoiding its detrimental embrittlement effect.

Titanium (Ti) and its alloys have been widely used in aerospace and biomedical industries owing to their superior specific strength, low elastic modulus, and corrosion resistance [1–3]. Among them, (α + β)-type Ti alloys composed of duplex phases are the most widely used ones due to their highly tunable microstructures and mechanical properties. By carefully manipulating the thermo-mechanical process, diverse microstructures including equiaxed grains, bimodal grain distribution, basketweave patterns, and Widmanstädter structure (martensite) can be engineered in the materials [3]. The equiaxed α + β dual-phase microstructure is highly attractive as it exhibits high ductility, high fatigue strength, and excellent impact toughness. However, it often displays mediocre strength due to the lack of additional strengthening mechanisms, such as solid-solution strengthening of α phase and precipitation strengthening of β phase. Alloying with complicated elements (including Al, Mo, V, Cr, Zr, etc.) and precipitation of fine acicular α phase by aging are usually mandatory to render the alloys with strength higher than 1200 MPa, which however increase both the material cost and fabrication cost [4–6]. Besides, the fine acicular α phase precipitated inside the β grain and at β grain boundary deteriorates ductility owing to the strain incompatibility between β matrix and α precipitates, thus premature fracture of the alloys [7–9]. It is still challenging to effectively harden the α + β dual-phase Ti alloys with fully equiaxed grains without substantially sacrificing ductility.

Oxygen as an interstitial element with a small atomic radius can create strong lattice distortion in Ti alloy, thus imparting significant strengthening [10,11]. However, it is documented that oxygen addition above 0.4 wt.% resulted in detrimental embrittlement in (α + β)-type Ti alloys with duplex phases [10,12,13]. The presence of oxygen inevitably depressed twinning activity [13,14] and promoted planar dislocation arrangement [12,13]. Besides, the enrichment of oxygen in the α phase due to the stronger affinity of the α phase with oxygen created distinct mechanical incompatibility between the α phase and β phase, which facilitated strain localization, crack initiation, and eventually premature failure of the materials [15]. *Chong* et al. [13] reported that oxygen sensitivity on ductility was mitigated in Ti-6Al-0.3O (wt.%) by promoting twinning and delocalizing dislocations, which substantially improved both cryogenic strength and ductility. The formation of basal texture in Ti-3Al-2Zr-2Mo-0.36O (wt.%) near-α alloy enhanced ductility

* Corresponding author.
E-mail address: wlxiao@buaa.edu.cn (W. Xiao).

https://doi.org/10.1016/j.scriptamat.2022.115236
Received 24 October 2022; Received in revised form 7 December 2022; Accepted 10 December 2022
Available online 13 December 2022

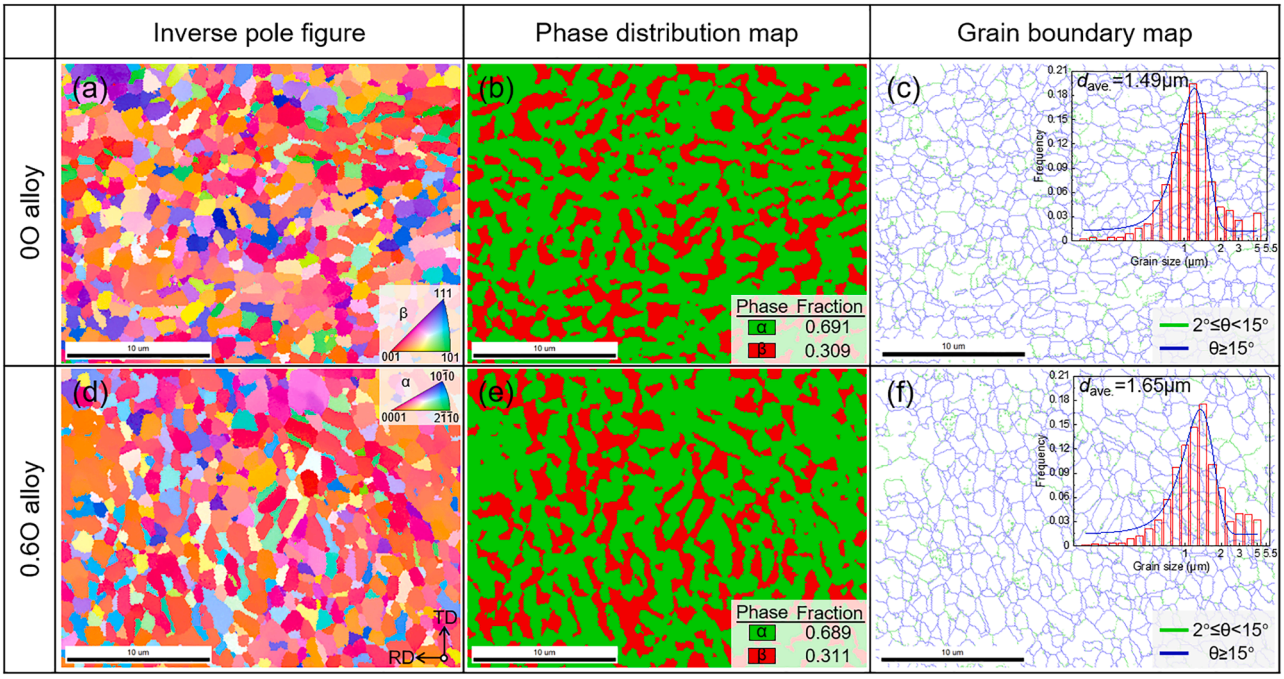

Fig. 1. EBSD images of the 0O and 0.6O alloys. The insets in (c) and (f) are corresponding grain size distribution histograms.

by promoting $\langle \boldsymbol{c}+\boldsymbol{a} \rangle$ slips [16]. It thus infers that the embrittlement in high oxygen-containing (α + β)-Ti alloys can be addressed through both compositional and microstructural design to initiate additional deformation modes in the α phase.

In this work, a 0.66 wt.% content of interstitial oxygen was elaborately doped to strengthen an (α + β)-type Ti-8Nb-2Fe-0.66O alloy (wt. %, Mo equivalent of 1.8) with fully equiaxed α + β microstructure. Taking full advantage of chemical composition and microstructure engineering, we reported for the first time the embrittlement dilemma in high oxygen-bearing (α + β)-Ti alloys was successfully addressed and ultrahigh tensile yield strength (1386 MPa) and good ductility (10.8%) were achieved.

The ingot with measured chemical composition of Ti-8.56Nb-2.08Fe-0.66O, referred to as 0.6O alloy hereafter, was prepared by vacuum arc melting using high-purity raw materials. Interstitial oxygen was doped by using TiO_2 powders. For comparison, a base alloy Ti-8.96Nb-2.5Fe-0.09O (0O alloy with Mo equivalent of 8.0) was also prepared. The ingots were remelted at least five times and heat-treated at 1000 °C for 2 h for chemical homogeneity. The chemical compositions of the alloys were measured by inductively coupled plasma-optical emission spectroscopy (ICP-OES) and a LECO ONH836 analyzer. For grain refinement, 10 mm thick plates cut from the ingots by electronic discharge machining were two-step hot-rolled, which was first rolled at 750 °C to 4 mm thick and then rolled at 650 °C to 1.5 mm thick sheets. Post-annealing was conducted at 725 °C for 30 min for recrystallization and then water quenched. Microstructure of the as-annealed specimens was observed by electron backscatter diffraction (EBSD) performed on a thermal field-emission scanning electron microscopy (SEM, Apreo S LoVac) and transmission electron microscopy (TEM, JEM-2100F) at an accelerating voltage of 200 kV. EBSD maps were obtained at 15 kV with a step size of 0.4 μm on the rolling plane. TEM samples were prepared by twin-jet polishing at 238 K using an electrolyte containing 5% perchloric acid, 35% methanol, and 60% normal butanol. Uniaxial tensile tests using dog-bone-shaped tensile specimens with gage sections of 18 mm × 5 mm × 1.5 mm at a strain rate of $5 \times 10^{-4}\ s^{-1}$ were conducted on an Instron-8801 testing system at room temperature, and the tests were repeated three times for reproducibility. Tensile direction was parallel to rolling direction and a strain extensometer was employed.

EBSD results in Fig. 1 reveal the formation of fully equiaxed fine grains consisting of α + β dual-phase with an average grain size of 1.65 μm of the 0.6O alloy. The phase distribution map (Fig. 1b) suggests that 68.9% of the grains are α phase with hexagonal close-packed (HCP) structure, in line with the XRD pattern (Supplementary Fig. S1). A strong basal texture in the α phase with $[0001]_\alpha$ *c*-axis nearly perpendicular to rolling plane was observed (Supplementary Fig. S2c), which originated from easy activation of basal slip during hot-rolling [17,18]. No apparent texture was observed in the β phase (Body-centered cubic, BCC) (Supplementary Fig. S2). The 0O alloy presents a highly similar microstructure to the 0.6O alloy as demonstrated in Fig. 1, Supplementary Figs. S1, and S2.

Bright-field (BF) TEM image (Fig. 2a) further confirmed the mixture of equiaxed α + β grains with β grains (darker contrast) almost isolated by the α matrix. No trace of oxides or intermetallic was observed. Dark-field (DF) TEM image in Fig. 2(b) illustrates the presence of nanoscale ω particles in the β phase. The formation of α + β dual-phase resulted in elemental redistribution [2], where β-stabilizers Nb and Fe were mostly partitioned to the β phase that enhanced the β phase stability and also hardened it, while O was enriched in α phase according to line scanning data (Supplementary Fig. S3). Above results suggest that oxygen showed minor influence on the microstructure of the base and 0.6O alloys. Nevertheless, the amount and size of the ω particles in the 0.6O alloy are lower than the base alloy (Supplementary Fig. S4) owing to the inhibition role of oxygen on the formation of athermal ω phase [19], which is beneficial for plastic deformation.

Despite the similarity in microstructure, the base alloy and 0.6O alloy exhibited largely different mechanical responses under tensile loading. The base alloy yielded (0.2% offset yielding) at low stress of 742 ± 7 MPa. Surprisingly, the yield strength of the 0.6O alloy was tremendously increased to 1386 ± 5 MPa while a relatively high ductility of 10.8 ± 0.6% was still maintained as shown in Fig. 3(a), successfully breaking the upper limit of 0.4 wt.% oxygen tolerance of ductility in (α + β)-Ti alloys [10]. The present 0.6O alloy possesses a superb combination of ultrahigh yield strength and good ductility that outperforms the α-type and (α + β)-type Ti alloys with fully equiaxed

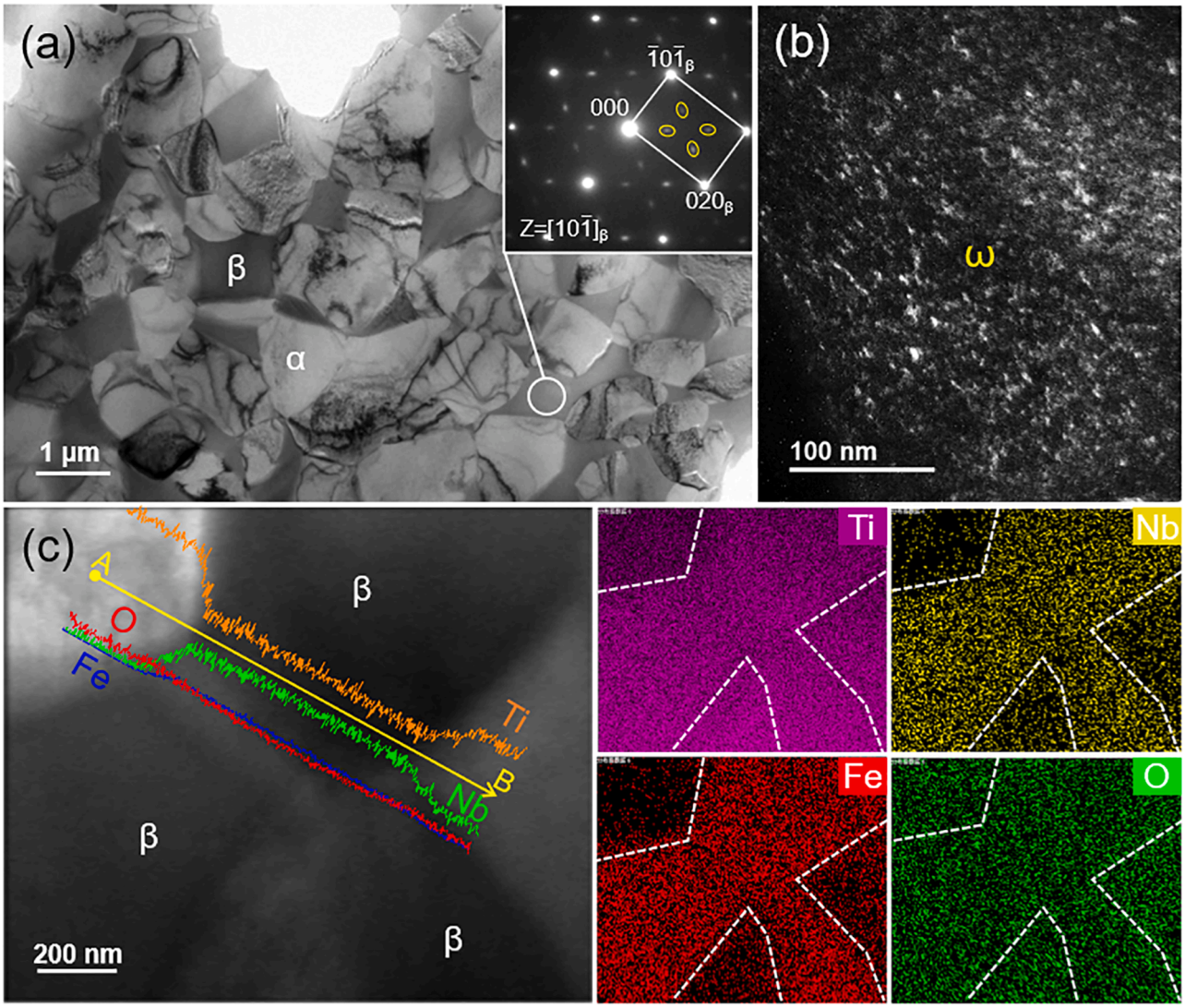

Fig. 2. TEM images of the 0.6O alloy. (a) BF image, the β and α grains are labeled by symbol β and α, respectively, (b) DF image of the athermal ω phase acquired by using the ellipses highlighted ω diffractions in the inset of (a), and (c) EDS elemental distribution maps with inset showing the line scanning results across A to B.

microstructure, and even superiors to other typical metastable β-type high-strength Ti alloys shown in Fig. 3(c). The change in mechanical properties is reflected by the evolution of strain hardening behaviors shown in Fig. 3(b). The rapid rise in strain hardening rate after elastic deformation indicates the presence of additional deformation modes that contributed to the maintained ductility [1,20,21]. A distinct yield drop phenomenon of the 0.6O alloy similar to steel and high entropy alloy with interstitial carbon [22] and oxygen [23] addition led to the noticeable drop in flow stress and strain hardening rate, which was a consequence of dislocations breaking up from the interstitial pinning. The strain hardening of the two alloys behaved similarly at strains higher than ~5%. The difference in strain hardening ability at low strain infers an alteration of deformation mode by oxygen addition, resulting in substantially enhanced yield strength of the 0.6O alloy.

To clarify the origin of the extraordinary high strength-ductility synergy of the 0.6O alloy, microstructure evolution after different tensile strains was investigated by TEM. Microstructure of the 0O alloy subjected to 5% strain is given in Fig. 4. Orthorhombic α" martensite (SIMα") formed by stress-induced β to α" martensitic transformation (SIMT) was observed in Fig. 4(a-c), which explains the high strain hardening rate of the base alloy at early plastic deformation through transformation-induced plasticity (TRIP) effect. The occurrence of SIMT indicates the metastable nature of the β phase. Besides, band-like structures along with dislocation tangle were observed in the α grain as seen in Fig. 4(d) and (f). These bands shared identical crystallographic structure with α-matrix but showed small yet noticeable local crystal rotation (Fig. 4e), thus are termed as α-kink bands [24]. These α-kink bands were initialized by extensive dislocation slipping that locally distorted and rotated the lattice, which acted as a stress-relaxation process to accommodate local stress concentration in the α phase, thus delaying crack initiation and imparting high ductility to the base alloy [25,26].

Microstructures of the 0.6O alloy subjected to 2%, 5%, and 10% tensile strains were shown in Fig. 5(a-c). No stress-induced phase transformation and deformation twinning were observed due to the inhabitation effect of oxygen [12,27]. Plastic deformation of the 0.6O alloy was thus accommodated by dislocation slipping, and the dislocation density increased with increasing strain. Dislocation density of the β phase was obviously lower than that of the α phase (Fig. 5a-c), inferring that the β phase was harder than the α phase. A $\boldsymbol{g.b}$ analysis shows that the dislocations observed in the α phase are primarily non-basal types and specifically prismatic $\langle \boldsymbol{a} \rangle$-type and pyramidal $\langle \boldsymbol{c}+\boldsymbol{a} \rangle$-type dislocations (Supplementary Fig. S5). Dislocations were first initiated at the α grains while leaving the β grains elastically deformed. The dislocations

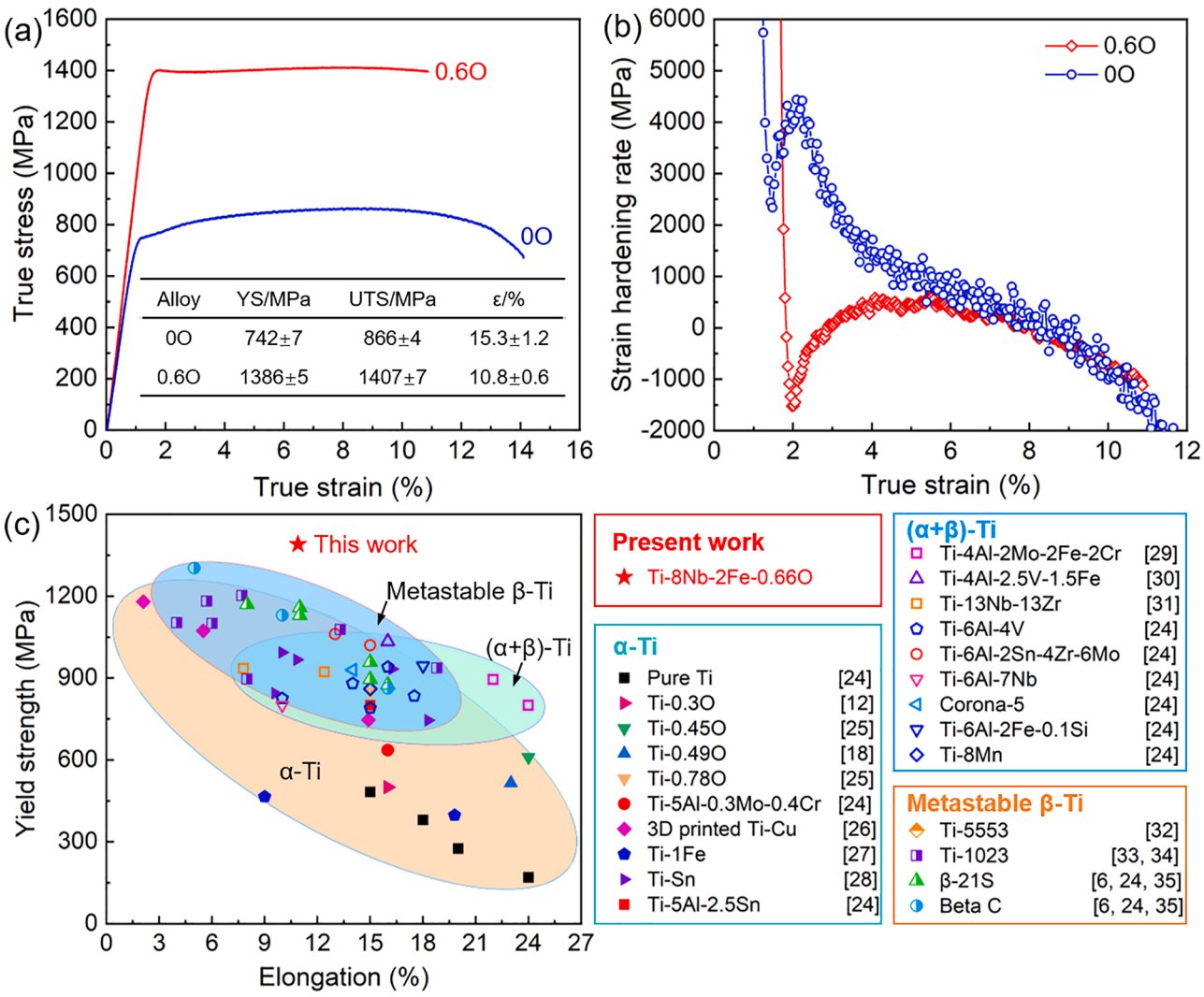

Fig. 3. Mechanical properties of the studied 0O and 0.6O alloys. (a) Tensile true stress-strain curves of the 0O and 0.6O alloys, the mechanical properties are summarized in the inset table where YS stands for yield strength, UTS for ultimate tensile strength, and ε for fracture elongation, (b) strain hardening rate curves corresponding to stress-strain curves in (a), and (c) comparison of yield strength and fracture elongation of the present 0.6O alloy with α-type (solid symbols), (α + β)-type (hollow symbols) and typical high-strength metastable β-Ti (half solid symbols) alloys [6,12,18,31,34–44].

at α grains then tangled and piled up at the α/β grain boundary with increasing strain, which generated stress concentration and then triggered dislocation slipping in the adjacent β grain [28], also known as heterogeneous deformation induced hardening [29]. Finally, a high density of dislocations piled up at α/β grain boundaries was encountered at high strain (Fig. 5c). The coordinate dislocation activities in α and β phases guaranteed good ductility of the 0.6O alloy, which was further confirmed by ductile fracture behavior and finer dimple size in Supplementary Fig. S7.

Results demonstrate a high tolerance of oxygen on the ductility of (α + β)-type Ti alloy with equiaxed microstructure. The formation of fine-grained α + β dual-phase architecture was beneficial for strength increment through grain refinement strengthening. However, as schematically illustrated in Fig. 5(d), the macroscopic yielding of the base alloy was dominated by SIMT of the β phase, resulting in low yield strength. Doping the base alloy with 0.66 wt.% oxygen together with β-stabilizers Nb and Fe strongly hardened the soft β phase. Therefore, plastic deformation of the 0.6O alloy was firstly accommodated by dislocation slipping in the α phase. The stress drop after onset of yielding indicates that dislocations temporally arrested by oxygen atoms were unpinned and therefore can glide on the slip planes, inferring that the strengthening mechanism was governed by interstitial solid-solution strengthening [23]. Interstitial oxygen atoms usually produce severe octahedral and tetragonal distortions in HCP lattice and BCC lattice, respectively. The strong but short-range repulsion interaction between screw dislocations and such lattice distortion centres substantially increased the critical resolved shear stress required for dislocation motion, thus hardening the materials [23,30]. Oxygen interstitial solid-solution strengthening of the α phase and β phase of the 0.6O alloy was calculated to be 590 MPa ($\Delta\sigma_\alpha$) and 732 MPa ($\Delta\sigma_\beta$), respectively (see Supplementary Materials). Hence, the theoretical yield strength increment ($\Delta\sigma_{YS}$) due to the doping of 0.66 wt.% oxygen was about 634 MPa according to the role of mixture: $\Delta\sigma_{YS} = 0.69\Delta\sigma_\alpha + 0.31\Delta\sigma_\beta$. This means that the experimental strengthening of yield strength by 644 MPa was mainly attributed to interstitial soli-solution strengthening. The above analysis indicates that the hardening of interstitial oxygen on the β phase was more pronounced as compared to the α phase caused by the severer tetragonal distortion [10], which reasoned the distinct lower dislocation density of the β phase at low applied strain (Fig. 5a and b).

Despite the substantially enhanced yield strength, the loss in ductility was marginal. The formation of equiaxed α + β dual-phase with strong basal α texture played a key role in causing multiple dislocation

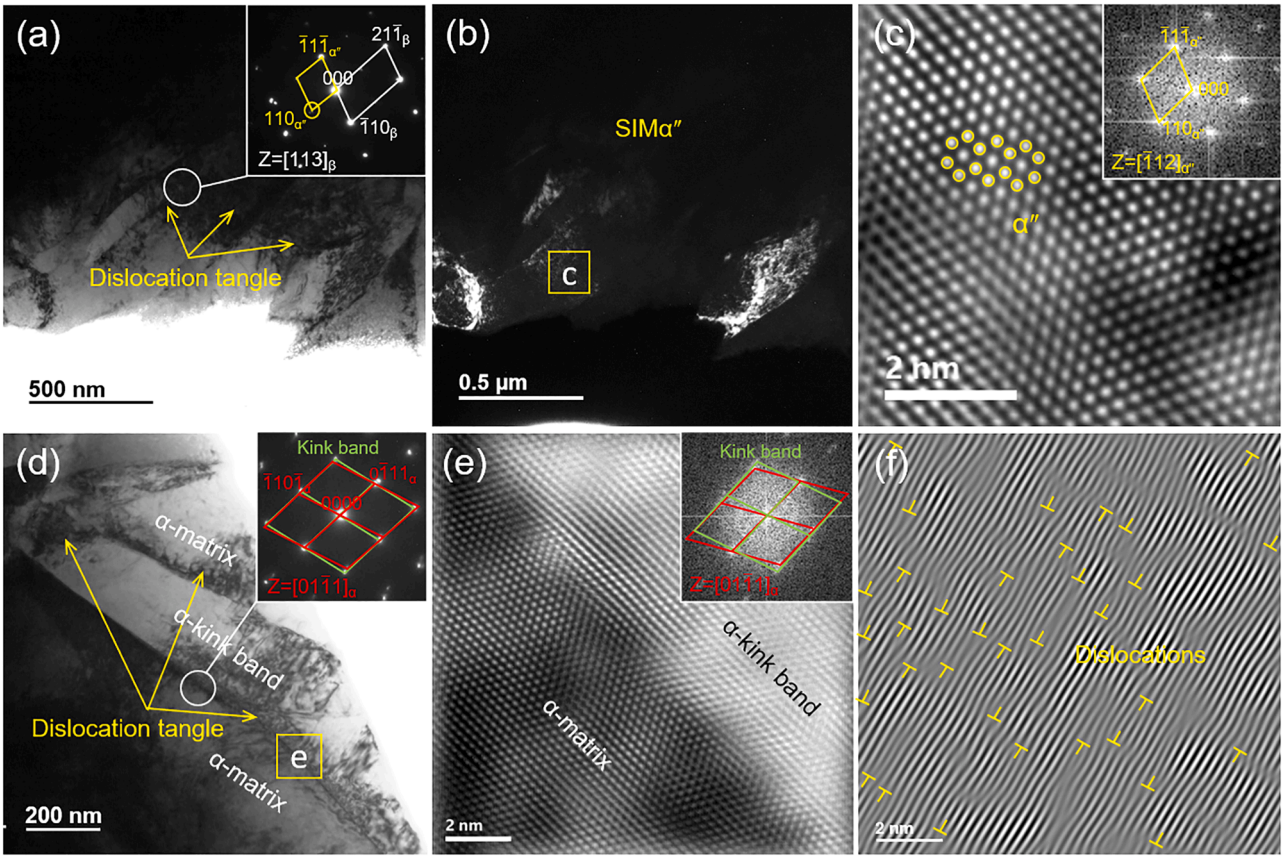

Fig. 4. TEM images of the 0O alloy after 5% tensile strain. (a) BF image of β matrix with inset showing SAED pattern of β matrix and SIMα", (b) DF image of the SIMα" using diffraction spot highlighted by the yellow circle in the inset of (a), (c) IFFT of the SIMα", (d) BF image of the α phase with inset SAED pattern recorded from the white circled area, (e) and (f) IFFT images showing the α-kink band and high-density dislocation accumulated around their interface, respectively.

activities, contributing to obtained good ductility. $\langle \boldsymbol{c}+\boldsymbol{a}\rangle$-type dislocations are essentially required to accomplish deformation along the *c*-axis of HCP crystal when twinning is absent. Basal α texture is beneficial for the activation of pyramidal $\langle \boldsymbol{a}\rangle$-type and $\langle \boldsymbol{c}+\boldsymbol{a}\rangle$-type dislocations according to Schmid factor maps (Supplementary Fig. S7) [16,31]. Note that the enhanced basal texture in the 0.6O alloy induced more favorable pyramidal and prismatic slips to maintain the ductility (Supplementary Fig. S2 and S7). The doping of interstitial oxygen also supported the $\langle \boldsymbol{c}+\boldsymbol{a}\rangle$ dislocations through an interstitial shuffling mechanism [28]. The equiaxed grains provided larger dislocation mean free path than fine acicular α, and the strong texture means a similar orientation between the adjacent α grains with respect to load direction, which favored dislocation transferring across different grains [32,33]. The $\langle \boldsymbol{c}+\boldsymbol{a}\rangle$ dislocations interacted with $\langle \boldsymbol{a}\rangle$ dislocations resulting in plenty of tangled dislocations and thus large strain hardening capability of the 0.6O alloy (Fig. 3b), delaying stress localization and crack initiation. The elaborately selected Nb, Fe β-stabilizers and interstitial oxygen substantially hardened the β phase, which minimize the mechanical incompatibility between equiaxed α and β grains. Both α and β phases accommodated plastic strain via dislocation slipping at the post deformation stage (Fig. 5c), which resulted in the almost identical strain hardening rate at strains higher than 5% and prolonged the ductility. Moreover, the reduction of the ω phase also contributed to the obtained good ductility. Consequently, the conventional undesired embrittlement effect of oxygen on (α + β)-Ti alloy was successfully overcome by coordinate dislocation slipping in both α and β phases.

In summary, results demonstrate that the oxygen tolerance on the ductility of (α + β)-type Ti alloys can be as high as 0.66 wt.%, which was achieved by the formation of equiaxed fine α + β dual-phase with basal α texture and activation of multiple dislocations in the α phase. Consequently, a superb combination of yield strength and ductility was realized by doping 0.66 wt.% oxygen interstitials. The remarkable increment in yield strength resulted from strong solid-solution hardening of both α and β phases and suppression of stress-induced β to α" martensitic transformation. The formation of equiaxed fine grains with strong basal α texture promoted $\langle \boldsymbol{c}+\boldsymbol{a}\rangle$ dislocations in the α phase, which in return contributed to the good ductility. Our results demonstrate a novel alloy design strategy for Ti alloys via engineering chemical composition and microstructure that turns the traditionally conceived detrimental oxygen interstitials into viable strengthening and toughening factors.

Declaration of Competing Interest

The authors declare that they have no known competing financial interests or personal relationships that could have appeared to influence the work reported in this paper.

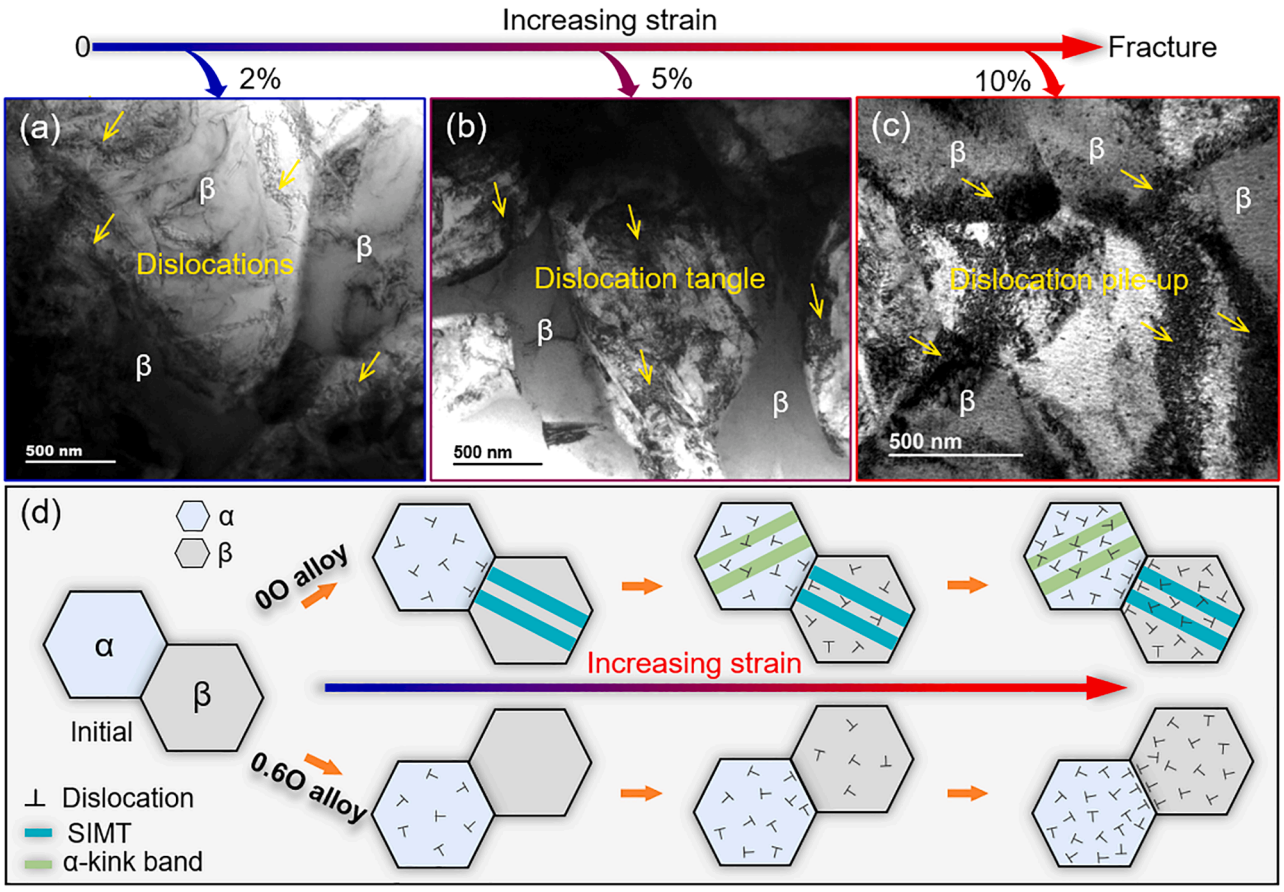

Fig. 5. BF-TEM images of the 0.6O alloy with different tensile strains. (a) 2%, (b) 5%, and (c) 10%. (d) Schematic illustration of the deformation mechanisms of the 0O and 0.6O alloys.

Acknowledgments

This work was financially supported by the National Natural Science Foundation of China (No. 51671012 and 52001018), the Youth Talent Support Program of Beihang University, and the China Aviation Development Independent Innovation Special Fund Project (CXPT-2020–033).

Supplementary materials

Supplementary material associated with this article can be found, in the online version, at doi:10.1016/j.scriptamat.2022.115236.

References

[1] S. Zhao, R. Zhang, Q. Yu, J. Ell, R.O. Ritchie, A.M. Minor, Cryoforged nanotwinned titanium with ultrahigh strength and ductility, Science 373 (2021) 1363–1368.

[2] P. Barriobero-Vila, J.M. Vallejos, J. Gussone, J. Haubrich, K. Kelm, A. Stark, N. Schell, G. Requena, Interface-mediated twinning-induced plasticity in a fine hexagonal microstructure generated by additive manufacturing, Adv. Mater. 33 (2021), 2105096.

[3] D. Banerjee, J.C. Williams, Perspectives on titanium science and technology, Acta Mater. 61 (2013) 844–879.

[4] L. Ren, W. Xiao, H. Chang, Y. Zhao, C. Ma, L. Zhou, Microstructural tailoring and mechanical properties of a multi-alloyed near beta titanium alloy Ti-5321 with various heat treatment, Mater. Sci. Eng: A 711 (2018) 553–561.

[5] W. Zhu, J. Lei, C. Tan, Q. Sun, W. Chen, L. Xiao, J. Sun, A novel high-strength β-Ti alloy with hierarchical distribution of α-phase: The superior combination of strength and ductility, Mater. Des. 168 (2019), 107640.

[6] J.D. Cotton, R.D. Briggs, R.R. Boyer, S. Tamirisakandala, P. Russo, N. Shchetnikov, J.C. Fanning, State of the art in beta titanium alloys for airframe applications, Miner. Metals Mat. Soc. 67 (2015) 1281–1303.

[7] B. Zhang, Y. Chong, R. Zheng, Y. Bai, R. Gholizadeh, M. Huang, D. Wang, Q. Sun, Y. Wang, N. Tsuji, Enhanced mechanical properties in β-Ti alloy aged from recrystallized ultrafine β grains, Mater. Des. 195 (2020), 109017.

[8] P. Li, Q. Sun, L. Xiao, J. Sun, Tuning the morphology of Ti-5Al-5Mo-5V-3Cr-1Zr alloy: From brittle to ductile fracture, Mater. Sci. Eng. A 769 (2020), 138487.

[9] T. Zhang, J. Zhu, T. Yang, J. Luan, H. Kong, W. Liu, B. Cao, S. Wu, D. Wang, Y. Wang, C.-.T. Liu, A new α + β Ti-alloy with refined microstructures and enhanced mechanical properties in the as-cast state, Scr. Mater. 207 (2022), 114260.

[10] M. Yan, W. Xu, M.S. Dargusch, H.P. Tang, M. Brandt, M. Qian, Review of effect of oxygen on room temperature ductility of titanium and titanium alloys, Powder Metall. 57 (2014) 251–257.

[11] X.-.Q. Wang, Y.-.S. Zhang, W.-.Z. Han, Design of high strength and wear-resistance β-Ti alloy via oxygen-charging, Acta Mater 227 (2022), 117686.

[12] Y. Chong, M. Poschmann, R. Zhang, S. Zhao, M.S. Hooshmand, E. Rothchild, D. L. Olmsted, J.W.M. Jr, D.C. Chrzan, M. Asta, A.M. Minor, Mechanistic basis of oxygen sensitivity in titanium, Sci. Adv. 6 (2020) 4060.

[13] Y. Chong, R. Zhang, M.S. Hooshmand, S. Zhao, D.C. Chrzan, M. Asta, J.W.M. Jr, A. M. Minor, Elimination of oxygen sensitivity in α-titanium by substitutional alloying with Al, Nat. Commun. 12 (2021) 6158.

[14] M. Morita, S. Suzuki, Y. Kato, W. Li, O. Umezawa, Tensile deformation of texture-controlled titanium with high oxygen content at room temperature, Mater. Sci. Eng. A 793 (2020), 139660.

[15] A. Zafari, K. Xia, High Ductility in a fully martensitic microstructure a paradox in a Ti alloy produced by selective laser melting, Mater. Res. Lett. 6 (2018) 627–633.

[16] H.R. Zhang, H.Z. Niu, S. Liu, M.C. Zang, D.L. Zhang, Significantly enhanced tensile ductility and its origin of a <0001>micro-textured extrusion bar of a powder metallurgy near alpha titanium alloy, Scr. Mater. 213 (2022), 114633.

[17] T.B. Britton, F.P.E. Dunne, A.J. Wilkinson, On the mechanistic basis of deformation at the microscale in hexagonal close-packed metals, Proc. R. Soc. A 471 (2015), 20140881.

[18] M. Tanaka, Y. Hayashi, Y. Okuyama, T. Morikawa, K. Higashida, Change in slip mode with temperature in Ti-0.49 mass%O, Mater. Trans. 60 (2019) 80–85.

[19] L.S. Wei, H.Y. Kim, T. Koyano, S. Miyazaki, Effects of oxygen concentration and temperature on deformation behavior of Ti-Nb-Zr-Ta-O alloys, Scr. Mater. 123 (2016) 55–58.

[20] M. Naeem, H. He, F. Zhang, H. Huang, S. Harjo, T. Kawasaki, B. Wang, S. Lan, Z. Wu, F. Wang, Y. Wu, Z. Lu, Z. Zhang, C.T. Liu, X.-.L. Wang, Cooperative deformation in high-entropy alloys at ultralow temperatures, Sci. Adv. 6 (2020) 4002.

[21] C. Herrera, D. Ponge, D. Raabe, Design of a novel Mn-based 1 GPa duplex stainless TRIP steel with 60% ductility by a reduction of austenite stability, Acta Mater 59 (2011) 4653–4664.
[22] B.B. He, B. Hu, H.W. Yen, G.J. Cheng, Z.K. Wang, H.W. Luo, M.X. Huang, High dislocation density-induced large ductility in deformed and partitioned steels, Science 357 (2017) 1029–1032.
[23] Z. Lei, X. Liu, Y. Wu, H. Wang, S. Jiang, S. Wang, X. Hui, Y. Wu, B. Gault, P. Kontis, D. Raabe, L. Gu, Q. Zhang, H. Chen, H. Wang, J. Liu, K. An, Q. Zeng, T.G. Nieh, Z. Lu, Enhanced strength and ductility in a high-entropy alloy via ordered oxygen complexes, Nature 563 (2018) 546–550.
[24] J. Zhang, B. Qian, Y. Wu, Y. Wang, J. Cheng, Z. Chen, J. Li, F. Sun, F. Prima, A kink-bands reinforced titanium alloy showing 1.3 GPa compressive yield strength: Towards extra high-strength/strain-transformable Ti alloys, J. Mater. Sci. Technol. 74 (2021) 21–26.
[25] S. Jin, K. Marthinsen, Y. Li, Formation of {11-21} twin boundaries in titanium by kinking mechanism through accumulative dislocation slip, Acta Mater. 120 (2016) 403–414.
[26] S. Yamasaki, T. Tokuzumi, W. Li, M. Mitsuhara, K. Hagihara, T. Fujii, H. Nakashima, Kink formation process in long-period stacking ordered Mg-Zn-Y alloy, Acta Mater. 195 (2020) 25–34.
[27] F.Q. Hou, S.J. Li, Y.L. Hao, R. Yang, Nonlinear elastic deformation behaviour of Ti-30Nb-12Zr alloys, Scr. Mater. 63 (2010) 54–57.
[28] Y. Chong, T. Tsuru, B. Guo, R. Gholizadeh, K. Inoue, N. Tsuji, Ultrahigh yield strength and large uniform elongation achieved in ultrafine-grained titanium containing nitrogen, Acta Mater. 240 (2022), 118411.
[29] Y. Zhu, X. Wu, Perspective on hetero-deformation induced (HDI) hardening and back stress, Mater. Res. Lett. 7 (2019) 393–398.
[30] Q. Yu, L. Qi, T. Tsuru, R. Traylor, D. Rugg, J.W.M. Jr, M. Asta, D.C. Chrzan, A. M. Minor, Origin of dramatic oxygen solute strengthening effect in titanium, Science 347 (2015) 635–639.
[31] J. Shen, B. Chen, J. Umeda, J. Zhang, Y. Li, K. Kondoh, An in-situ study on deformation and cracking initiation in oxygen-doped commercial purity titanium, Mech. Mater. 148 (2020), 103519.
[32] S. Wei, G. Zhu, C.C. Tasan, Slip-twinning interdependent activation across phase boundaries: An in-situ investigation of a Ti-Al-V-Fe (α+β) alloy, Acta Mater. 206 (2021), 116520.
[33] K. Chen, H. Li, D.J. Huang, X. Shen, N. Jia, Avoiding oxygen-induced early fracture in titanium with high strength via entangled grains through laser powder bed fusion, Scr. Mater. 222 (2023), 115051.
[34] I. Polmear, D. StJohn, J.-.F. Nie, M. Qian, Titanium Alloys, Butterworth-Heinemann, Oxford, 2017.
[35] D. Zhang, D. Qiu, M.A. Gibson, Y. Zheng, H.L. Fraser, D.H. StJohn, M.A. Easton, Additive manufacturing of ultrafine-grained high-strength titanium alloys, Nature 576 (2019) 91–95.
[36] Y. Chong, R. Zheng, G. Deng, A. Shibata, N. Tsuji, Investigation on the microstructure and mechanical properties of Ti-1.0Fe alloy with equiaxed α + β microstructures, Metall. Mater. Trans. A 51 (2020) 2851–2862.
[37] X.X. Ye, B. Chen, J.H. Shen, J. Umeda, K. Kondoh, Microstructure and strengthening mechanism of ultrastrong and ductile Ti-xSn alloy processed by powder metallurgy, J. Alloy. Compd. 709 (2017) 381–393.
[38] S.W. Lee, J.H. Kim, C.H. Park, J.-.K. Hong, J.-.T. Yeom, Alloy design of metastable α+β titanium alloy with high elastic admissible strain, Mater. Sci. Eng. A 802 (2020), 140621.
[39] S. Wei, J. Kim, C.C. Tasan, In-situ investigation of plasticity in a Ti-Al-V-Fe (α+β) alloy: Slip mechanisms, strain localization, and partitioning, Inter. J. Plast. 148 (2022), 103131.
[40] T. Lee, K.-.T. Park, D.J. Lee, J. Jeong, S.H. Oh, H.S. Kim, C.H. Park, C.S. Lee, Microstructural evolution and strain-hardening behavior of multi-pass caliber-rolled Ti-13Nb-13Zr, Mater. Sci. Eng. A 648 (2015) 359–366.
[41] J.C. Fanning, Properties of TIMETAL 555 (Ti-5Al-5Mo-5V-3Cr-0.6Fe), J. Mater. Eng. Perform. 14 (2005) 788–791.
[42] Y. Danard, R. Poulain, M. Garcia, R. Guillou, D. Thiaudière, S. Mantri, R. Banerjee, F. Sun, F. Prima, Microstructure design and in-situ investigation of TRIP/TWIP effects in a forged dual-phase Ti-10V-2Fe-3Al alloy, Materialia 8 (2019), 100507.
[43] Y. Chong, S. Gao, N. Tsuji, A unique three-stage dependence of yielding behavior and strain-hardening ability in Ti-10V-2Fe-3Al alloy on phase fraction, Mater. Sci. Eng. A 821 (2021), 141609.
[44] S.L. Nyakana, J.C. Fanning, R.R. Boyer, Quick reference guide for β titanium alloys in the 00 s, J. Mater. Eng. Perform. 14 (2005) 799–811.